

# Study of the ferromagnetic-insulator phase in manganites

Sanjukta Paul and Sudhakar Yarlagadda

*CMP Div., Saha Institute of Nuclear Physics, HBNI, Kolkata, India*

(Dated: June 7, 2021)

Understanding the coexistence of ferromagnetism and insulating behavior in manganites is an unsolved problem. We propose a localized-band model involving effective intermediate-range electron-electron (electron-hole) repulsion (attraction) generated by cooperative electron-phonon interaction. Double exchange mechanism, involving holes virtually hopping to nearest neighbors and back, produces magnetic polarons in an antiferromagnetic environment; when these magnetic polarons coalesce and percolate the system, we get a ferromagnetic insulator. Ferromagnetism gets more pronounced when the holes (doping) increases or when the ratio hopping/polaronic-energy dominates over superexchange-coupling/hopping.

PACS numbers: 75.85.+t, 71.38.-k, 71.45.Lr, 71.38.Ht, 75.47.Lx, 75.10.-b

## I. INTRODUCTION

Perovskite oxides, such as manganites, display a variety of orbital, charge, and spin orders when the parent oxide is doped. While significant progress has been made in characterizing most of the phenomena in bulk doped materials, the understanding pertaining to ferromagnetic insulator is still elusive. The doped alloy  $T_{1-x}D_xMnO_3$  (where T refers to trivalent rare-earth elements such as La, Pr, Nd, etc. and D refers to divalent alkaline elements Sr, Ca, etc.) is an antiferromagnet when  $x > 0.5$  with the nature of the antiferromagnet (i.e., A-, C-, CE-, or G-type antiferromagnet) depending on the compound and the dopant value  $x^{1-3}$ . Contrastingly, for  $x < 0.5$ ,  $T_{1-x}D_xMnO_3$  is an intriguing ferromagnetic insulator (FMI) at smaller values of  $x$  (i.e.,  $0.1 \lesssim x \lesssim 0.2$ )<sup>4-6</sup> and is a ferromagnetic metal at higher dopings in the manganite systems  $La_{1-x}Sr_xMnO_3$ ,  $La_{1-x}Ca_xMnO_3$ ,  $Pr_{1-x}Sr_xMnO_3$ , and  $Nd_{1-x}Sr_xMnO_3$ .

For modeling the diverse orderings and for exploiting the functionality in these transition-metal oxides, one needs effective Hamiltonians for various types of interactions. Although the importance of strong electron-phonon interaction (EPI) has been pointed much earlier<sup>7</sup> and significant progress has been made some time ago in numerically treating electron-phonon interaction in sizeable systems<sup>8</sup>, the treatment of cooperative EPI (involving quantum phonons) was accomplished analytically only more recently in two dimensions (2D)<sup>9</sup>. It has been demonstrated analytically in Ref. 9 that introducing cooperative effects, when EPI is strong, produces nearest-neighbor (NN), next-nearest-neighbor (NNN), and next-to-next-nearest-neighbor (NNNN) interactions. Furthermore, incorporating spin-spin interactions along with cooperative strong EPI is still an unsolved analytic problem.

As regards experiments pertaining to ferromagnetic-insulating regions, while some suggested microscopically homogeneous electronic properties<sup>10-12</sup>, others speculate that coexistence of ferromagnetic metallic phases and antiferromagnetic insulating phases leads to an inhomogeneous ferromagnetic insulating state<sup>13,14</sup>.

We will now argue, without considering any specific model, that ferromagnetic insulating phases are possible at low doping in manganites by presenting below general theoretical points based on the essential features of manganites.

1) Kinetic energy (KE) is quite small at low doping because bare hopping is small (caused by lower tolerance factor<sup>15</sup>, cation disorder, compatibility of distortions<sup>16</sup>), and the electron-phonon coupling is strong.

2) Potential energy [from repulsive interactions, due to cooperative EPI, that are intermediate-range, i.e., NN, NNN, NNNN, etc.] is much larger than KE; this leads to solid-type formation with electrons being rendered essentially immobile and site localized. The ground state is classical and the state of the system can be expressed by a single state in the occupation number basis with number density at each site either 1 or 0.

The fact that electrons are essentially site localized also follows from the treatment in Ref. 17; then, only a localized polaronic band is relevant and the upper wide band cannot overlap with the lower narrow polaronic band.

Furthermore, a simple type of phase separated state with ferromagnetic droplets (each containing one carrier) in an antiferromagnetic matrix was shown to be possible in Ref. 18. The mobility of these magnetic polarons is low and they are easily localized by disorder and Coulomb interactions.

Thus the potential energy determines the charge and spin order.

3) Because of cooperative strong EPI, a NN electron-hole pair has a strong ferromagnetic interaction [ $t^2 \cos^2(\theta/2)/(2E_{JT})$  with  $E_{JT}$  being the cooperative Jahn-Teller energy,  $t$  the hopping term between the NN sites, and  $\theta$  the angle between the NN core spins]. Hence, a robust ferromagnetic cluster is produced in the vicinity of a hole.

4) Our model for magnetic interaction applies to manganites with low density of localized holes. In regions away from the holes, the cooperative EPI retains essentially the same orbital texture as in the undoped manganite. As a result, in regions without holes, the magnetic interaction is A-AFM just as in the undoped manganite. As regards

the regions with holes, since the holes are site localized, the holes only virtually hop to a NN site and back and thus produce ferromagnetic coupling with NN electrons. This ferromagnetic coupling, between NN electron-hole pair, is much stronger than A-AFM coupling.

5) Presence of site localized holes produces FMI clusters due to formation of magnetic polarons. A hole will polarize NN electrons (and realistically speaking, NNN and NNNN electrons as well) through virtual hopping, thereby producing a magnetic polaron. A collection of interacting magnetic polarons will produce a FMI region. It is interesting to note that FMI regions are present at moderate doping in manganites that are narrow band ( $\text{Pr}_{1-x}\text{Ca}_x\text{MnO}_3$ ), intermediate band ( $\text{La}_{1-x}\text{Ca}_x\text{MnO}_3$ ) and wide band ( $\text{La}_{1-x}\text{Sr}_x\text{MnO}_3$ ).

Rest of the paper is organized as follows. In Sec. II, invoking cooperative electron-phonon-interaction physics, we obtain the effective Hamiltonian that is employed to understand the FMI phase in manganites. Next, in Sec. III, we outline our calculation procedure involving Monte Carlo technique, used to simulate charge and spin configurations, and obtain the magnetization as a function of various parameters. Then, in Sec. IV, we discuss our results obtained for systems with different hoppings at different temperatures and dopings. Lastly, in Sec. V, we conclude and offer some perspectives.

## II. EFFECTIVE HAMILTONIAN

In this section we focus on the analytical treatment of the effective Hamiltonian which will be used for numerical simulation. We are working with a 2D version of the perovskite manganite system which has Mn-O-Mn bonds along the  $x$  and  $y$  directions. We have  $e_g$  electrons (or holes) interacting with the oxygen atoms. We have restricted our analysis to a system of fermions interacting with the oxygens in the  $xy$ -plane via cooperative breathing mode and with the out-of-plane  $z$ -direction oxygens through non-cooperative breathing mode as depicted in Fig. 1.

Apart from the itinerant  $e_g$  electrons, we also have a  $t_{2g}$  localized core-spin background; the large  $S = 2$  spin (comprising of contribution from a  $e_g$  spin and three  $t_{2g}$  spins) at each site is considered classical. Thus the Hamiltonian of such a system has four interactions: the kinetic energy of the fermions, the fermion-lattice coupling energy, the lattice energy, and the spin-spin interaction energy.

$$H = H_{\text{KE}} + H_{\text{int}} + H_{\text{lat}} + H_{\text{SE}}. \quad (1)$$

Here,

$$H_{\text{KE}} = -t \sum_{i,j} \left[ \cos\left(\frac{\theta_{i,j;i+1,j}}{2}\right) d_{i+1,j}^\dagger d_{i,j} + \cos\left(\frac{\theta_{i,j;i,j+1}}{2}\right) d_{i,j+1}^\dagger d_{i,j} + \text{H.c.} \right], \quad (2)$$

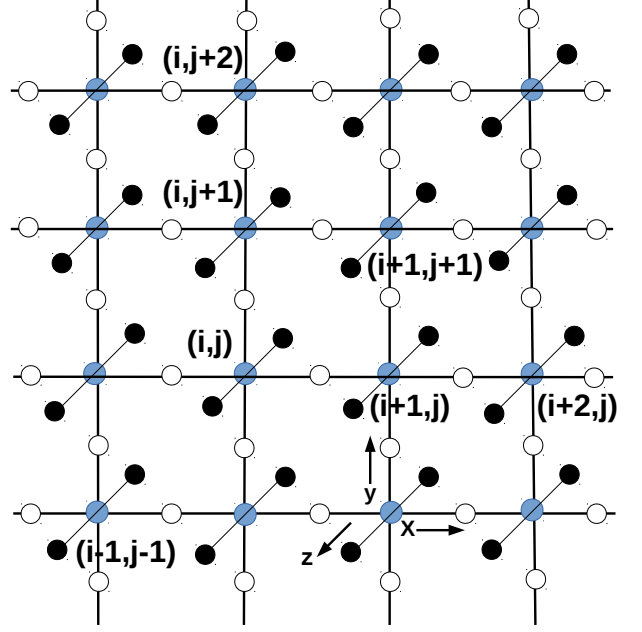


FIG. 1. (Color online) Schematic diagram for a 2D cooperative breathing mode (CBM) system. Hopping sites for holes are represented by blue solid circles, in-plane oxygen atoms (participating in the CBM) by black empty circles, and non-cooperative out-of-plane oxygen atoms by solid black circles.

and  $d_{i,j}$  ( $d_{i,j}^\dagger$ ) represents the annihilation (creation) operator for the fermion at site  $(i,j)$ ;  $t$  is the hopping amplitude for the fermion; the hopping process is modified by  $\theta$ , the angle between two spins at NN sites.<sup>25,26</sup> The second term represents the interaction between the fermions and the quantum phonons in the system and is expressed as<sup>9</sup>

$$H_{\text{int}} = -g\omega_0 \sum_{i,j} \left\{ (a_{x;i,j}^\dagger + a_{x;i,j}) (n_{i,j} - n_{i+1,j}) + (b_{y;i,j}^\dagger + b_{y;i,j}) (n_{i,j} - n_{i,j+1}) + \gamma (c_{z;i,j}^\dagger + c_{z;i,j}) n_{i,j} \right\}, \quad (3)$$

where  $\gamma = \sqrt{2}$ ,  $g$  is the electron-fermion coupling constant,  $\omega_0$  is the optical-phonon frequency, and  $n_{i,j} = d_{i,j}^\dagger d_{i,j}$ . The displacement of the oxygen atom that is adjacent to the site  $(i,j)$  in the positive  $x$  [ $y$ ] direction is given by  $\frac{(a_{x;i,j}^\dagger + a_{x;i,j})}{\sqrt{2m\omega_0}}$  [ $\frac{(b_{y;i,j}^\dagger + b_{y;i,j})}{\sqrt{2m\omega_0}}$ ]. In the  $z$  direction, the relative displacement of the two oxygen atoms next to site  $(i,j)$  is denoted by  $\frac{(c_{z;i,j}^\dagger + c_{z;i,j})}{\sqrt{2m\omega_0/2}}$  with  $m/2$  being the reduced mass of the oxygen pair. Next, the lattice energy due to quantum harmonic oscillators is given by

$$H_{\text{lat}} = \sum_{i,j} \left( a_{x;i,j}^\dagger a_{x;i,j} + b_{y;i,j}^\dagger b_{y;i,j} + \eta c_{z;i,j}^\dagger c_{z;i,j} \right), \quad (4)$$

with  $\eta$  being set to be 1.

Now, to arrive at an effective Hamiltonian which can be expressed solely in terms of fermionic operators, we take resort to an analytic approach similar to that described in<sup>9</sup>. For large electron-phonon coupling and restricting the system to the non-adiabatic regime,  $t/\omega_0 \lesssim 1$ , the above Hamiltonian  $H$  is subject to a canonical transformation (i.e., modified Lang-Firsov transformation) to produce an unperturbed part  $H_0$  and the perturbation term  $H_1$ . To obtain an effective Hamiltonian, we perform second-order perturbation theory (as in Refs. 9 and 28) and obtain

$$\begin{aligned}
H_{\text{eff}} = & -E_p \sum_{i,j} n_{i,j} + 2V_p \sum_{i,j} \left( n_{i,j} n_{i+1,j} + n_{i,j} n_{i,j+1} \right) \\
& + t e^{-(E_p+V_p)/\omega_0} \sum_{i,j} \left[ \cos \left( \frac{\theta_{i,j;i+1,j}}{2} \right) d_{i+1,j}^\dagger d_{i,j} \right. \\
& \left. + \cos \left( \frac{\theta_{i,j;i,j+1}}{2} \right) d_{i,j+1}^\dagger d_{i,j} + \text{H.c.} \right] \\
& + H^{(2)} + H_{\text{SE}}, \tag{5}
\end{aligned}$$

where the polaronic energy  $E_p = (4 + \gamma^2)g^2\omega_0 = 6g^2\omega_0$  and the nearest-neighbor repulsion energy  $V_p = g^2\omega_0$ ; the second order perturbation theory yields the term  $H^{(2)}$ . The small parameter of the perturbation theory is  $\sim \left[ \frac{t^2}{2(E_p+V_p)\omega_0} \right]^{\frac{1}{2}}$  as derived in Ref. 29. Now, the effective hopping term  $t e^{-(E_p+V_p)/\omega_0} \ll \omega_0$ . For large  $g$ , the effective hopping term will be very small compared to the other terms in  $H_{\text{eff}} - H_{\text{SE}}$ . Hence, we ignore the kinetic energy of the system and treat the system as made up of carriers that are localized due to disorder. Then, we are justified in treating the problem entirely classically with physics being governed by the dominant potential energy terms in the effective Hamiltonian. The first term

of  $H_{\text{eff}}$  can as well be represented in terms of electron-hole attraction instead of fermion-fermion repulsion. In general

$$\begin{aligned}
V_p \sum_{i,j,\delta} n_{i,j} n_{i+\delta,j} = & -V_p \sum_{i,j,\delta} n_{i,j} (1 - n_{i+\delta,j}) \\
& + V_p \sum_{i,j,\delta} n_{i,j}. \tag{6}
\end{aligned}$$

This formalism adds a constant energy term  $V_p \sum_{i,j,\delta} n_{i,j}$  to the Hamiltonian and thus does not change the physics of the problem. Then, using Eq. (6) we can rewrite Eq. (5) as

$$\begin{aligned}
H_{\text{eff}} = & -E_p \sum_{i,j} n_{i,j} - 2V_p \sum_{i,j} \left\{ n_{i,j} (1 - n_{i+1,j}) \right. \\
& \left. + n_{i,j} (1 - n_{i,j+1}) \right\} + 4V_p \sum_{i,j} n_{i,j} \\
& + H^{(2)} + H_{\text{SE}}. \tag{7}
\end{aligned}$$

The convention we will use throughout the paper is that  $n_{i,j}$  will represent number density of a hole at the lattice site  $(i, j)$  of the system. To calculate  $H^{(2)}$ , we go through an algebra similar to that mentioned in Appendix A of Ref. 9 and arrive at a nearest-neighbor repulsion term corresponding to the process where a particle in 2D virtually hops to its NN and comes back. When a hole at site  $(i, j)$  hops to its NN site, such as  $(i+1, j)$ , and comes back, we need to keep track of the occupancy of the three relevant nearest-neighbor sites of the intermediate site  $(i+1, j)$ , i.e., the occupancy of the three sites  $(i+2, j)$ ,  $(i+1, j+1)$  and  $(i+1, j-1)$ . Depending on how many of these three sites are filled, the coefficient for the hopping-and-returning process will be modified.

Clearly, there are four such possibilities for the coefficients and they will be considered below.

### A. Three NN sites of the intermediate site are filled by electrons.

In Fig. 2, when the intermediate site containing an electron is surrounded by a hole and three electrons, we depict the hole at site  $(i, j)$  hopping to its NN site (the intermediate site) and returning back. The intermediate site can be any of the four NNs of the originating site  $(i, j)$ . A schematic view of the four possibilities is shown in Fig. 2.

When a hole is at  $(i, j)$ , its energy is equal to  $-E_p$ . The oxygen atoms on both the sides of the initial site are attracted by the hole on the initial site and hence are pulled towards the hole. When the hole virtually hops to the intermediate site, its energy is equal to  $E_p + 2V_p$  because the oxygen distortions remain unchanged; in the energy of the intermediate state,  $E_p$  arises due to the distortion without the hole whereas the extra energy  $2V_p$  (equal in magnitude to the NN repulsion energy between two holes) results due to displacing the oxygen atoms towards the initial site and away from the hole. Hence, change in the energy when the hole jumps from the originating site to the intermediate site is equal to  $2E_p + 2V_p$ . Thus, the coefficient of the second order perturbation term turns out to be

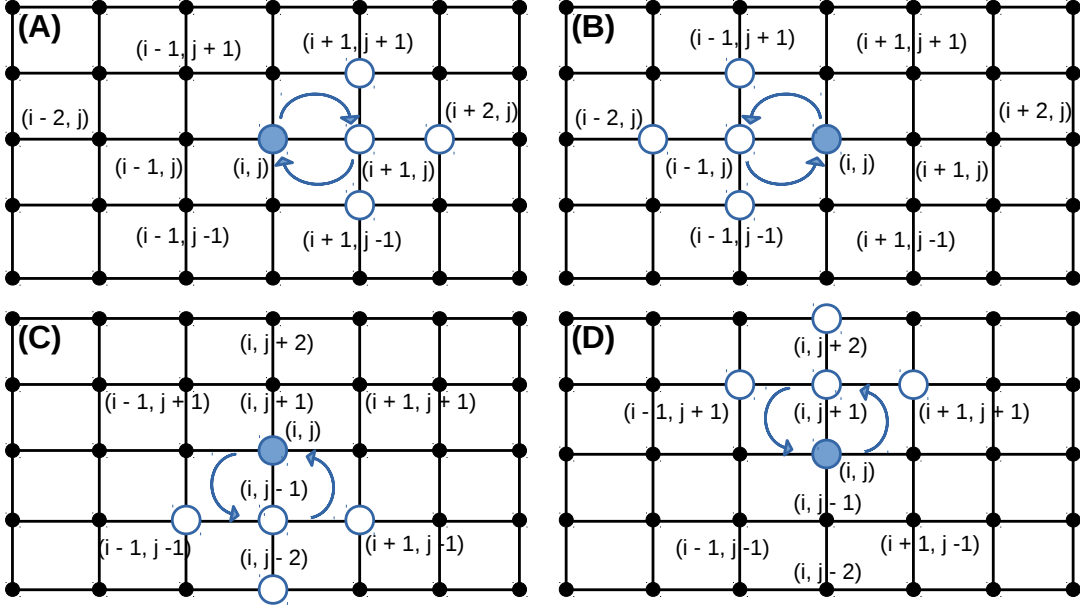


FIG. 2. (Color online) Schematic diagram for the four possibilities of a hole, at an originating site  $(i, j)$ , hopping to its NN site (the intermediate site) and coming back (when three NN sites of the intermediate site are occupied by electrons): (A) hole at  $(i, j)$  hops to its right NN at  $(i+1, j)$  and comes back; (B) hole at  $(i, j)$  jumps to its left NN at  $(i-1, j)$  and returns back; (C) hole at  $(i, j)$  jumps to its downward NN at  $(i, j-1)$  and comes back; (D) hole at  $(i, j)$  hops to its upper NN at  $(i, j+1)$  and returns. A hole is represented by a blue solid circle and a particle (i.e., electron) by a blue empty circle. All lattice sites that are not relevant to the consideration are represented by black solid circles.

$\frac{t^2}{2E_p+2V_p}$  and the contribution to  $H^{(2)}$  from all the possibilities corresponding to Fig. 2 is given by

$$\begin{aligned}
H_1^{(2)} = & -\frac{t^2}{(2E_p+2V_p)} \sum_{i,j} \left[ \cos^2 \left( \frac{\theta_{i,j;i+1,j}}{2} \right) \left\{ n_{i,j}(1-n_{i+1,j})(1-n_{i+2,j})(1-n_{i+1,j+1})(1-n_{i+1,j-1}) \right\} \right. \\
& + \cos^2 \left( \frac{\theta_{i,j;i-1,j}}{2} \right) \left\{ n_{i,j}(1-n_{i-1,j})(1-n_{i-2,j})(1-n_{i-1,j+1})(1-n_{i-1,j-1}) \right\} \\
& + \cos^2 \left( \frac{\theta_{i,j;i,j+1}}{2} \right) \left\{ n_{i,j}(1-n_{i,j+1})(1-n_{i,j+2})(1-n_{i-1,j+1})(1-n_{i+1,j+1}) \right\} \\
& \left. + \cos^2 \left( \frac{\theta_{i,j;i,j-1}}{2} \right) \left\{ n_{i,j}(1-n_{i,j-1})(1-n_{i,j-2})(1-n_{i-1,j-1})(1-n_{i+1,j-1}) \right\} \right]. \quad (8)
\end{aligned}$$

### B. Any two of NN sites of the intermediate site is filled.

In Fig. 3, we depict the three possibilities corresponding to a hole at a site  $(i, j)$  hopping to its NN site (the intermediate site) and returning; here, any two of the NN sites of the intermediate site are occupied by electrons. Henceforth, we will show all the counterpart processes of Fig. 2(A) (considering these as representative diagrams) for various possibilities. Similar processes, which will not be shown here, also occur for Fig. 2(B), Fig. 2(C), and Fig. 2(D).

When the hole virtually hops to the intermediate site, its energy is equal to  $E_p + 4V_p$ ; here, an extra repulsion of  $2V_p$  is generated due to the occupancy of any one of the NN site of the intermediate site by a hole. Then, the coefficient of the second order perturbation term is  $\frac{t^2}{2E_p+4V_p}$  and the contribution to  $H^{(2)}$  from all the possibilities, similar to and corresponding to Fig. 3, is given by

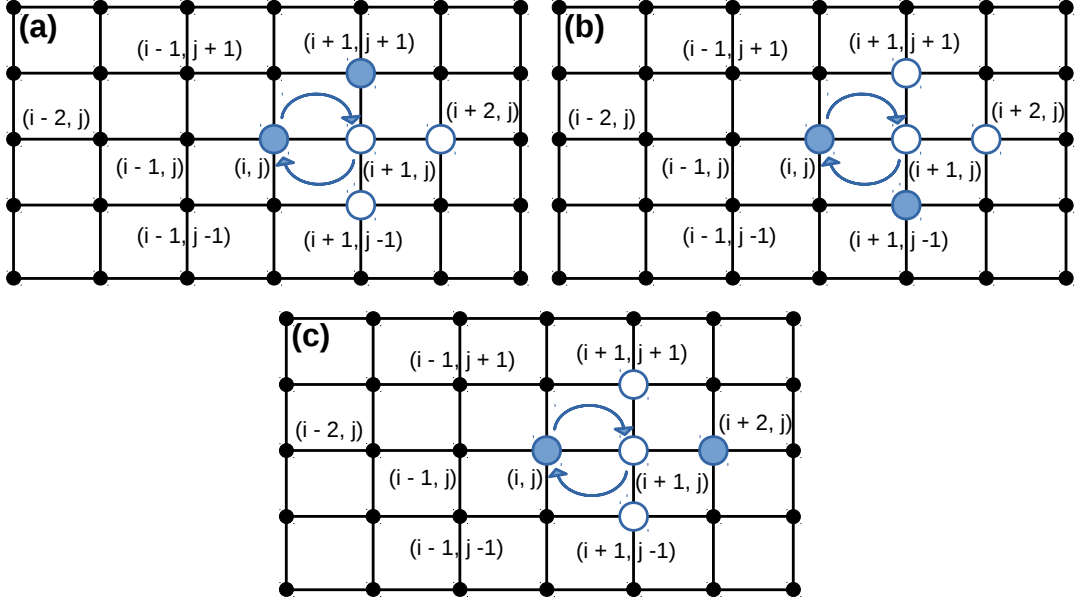


FIG. 3. (Color online) Schematic diagram for a hole at an originating site  $(i, j)$  hopping to its NN site (the intermediate site) and returning back (when any two of the NN sites of the intermediate site are occupied by electrons). Representation of a hole at  $(i, j)$  jumping to its right NN at  $(i + 1, j)$  and coming back when holes occupy (a) right and downward NNs of the intermediate site; (b) right and upward NNs of the intermediate site; (c) upward and downward NNs of the intermediate site. A hole is depicted by a blue solid circle and a particle by a blue empty circle. All lattice sites that are not relevant to the consideration are represented by black solid circles.

$$\begin{aligned}
H_2^{(2)} = & -\frac{t^2}{(2E_p + 4V_p)} \sum_{i,j} \left[ \cos^2 \left( \frac{\theta_{i,j;i+1,j}}{2} \right) \left\{ n_{i,j}(1 - n_{i+1,j})n_{i+2,j}(1 - n_{i+1,j+1})(1 - n_{i+1,j-1}) \right. \right. \\
& + n_{i,j}(1 - n_{i+1,j})(1 - n_{i+2,j})n_{i+1,j+1}(1 - n_{i+1,j-1}) + n_{i,j}(1 - n_{i+1,j})(1 - n_{i+2,j})(1 - n_{i+1,j+1})n_{i+1,j-1} \left. \right\} \\
& + \cos^2 \left( \frac{\theta_{i,j;i-1,j}}{2} \right) \left\{ n_{i,j}(1 - n_{i-1,j})n_{i-2,j}(1 - n_{i-1,j+1})(1 - n_{i-1,j-1}) \right. \\
& + n_{i,j}(1 - n_{i-1,j})(1 - n_{i-2,j})n_{i-1,j+1}(1 - n_{i-1,j-1}) + n_{i,j}(1 - n_{i-1,j})(1 - n_{i-2,j})(1 - n_{i-1,j+1})n_{i-1,j-1} \left. \right\} \\
& + \cos^2 \left( \frac{\theta_{i,j;i,j+1}}{2} \right) \left\{ n_{i,j}(1 - n_{i,j+1})n_{i,j+2}(1 - n_{i-1,j+1})(1 - n_{i+1,j+1}) \right. \\
& + n_{i,j}(1 - n_{i,j+1})(1 - n_{i,j+2})n_{i-1,j+1}(1 - n_{i+1,j+1}) + n_{i,j}(1 - n_{i,j+1})(1 - n_{i,j+2})(1 - n_{i-1,j+1})n_{i+1,j+1} \left. \right\} \\
& + \cos^2 \left( \frac{\theta_{i,j;i,j-1}}{2} \right) \left\{ n_{i,j}(1 - n_{i,j-1})n_{i,j-2}(1 - n_{i-1,j-1})(1 - n_{i+1,j-1}) \right. \\
& + n_{i,j}(1 - n_{i,j-1})(1 - n_{i,j-2})n_{i-1,j-1}(1 - n_{i+1,j-1}) \\
& \left. + n_{i,j}(1 - n_{i,j-1})(1 - n_{i,j-2})(1 - n_{i-1,j-1})n_{i+1,j-1} \right\} \Big]. \tag{9}
\end{aligned}$$

### C. Any one of NN sites of the intermediate site has an electron.

In Fig. 4, three possibilities have been shown for the process where a hole jumps to an intermediate site and comes back; here, any one of the NNs of the intermediate site is filled by an electron. Extending the logic given above to the present case, the coefficient of the second order perturbation term is  $\frac{t^2}{2E_p + 6V_p}$  and the contribution to  $H^{(2)}$  from

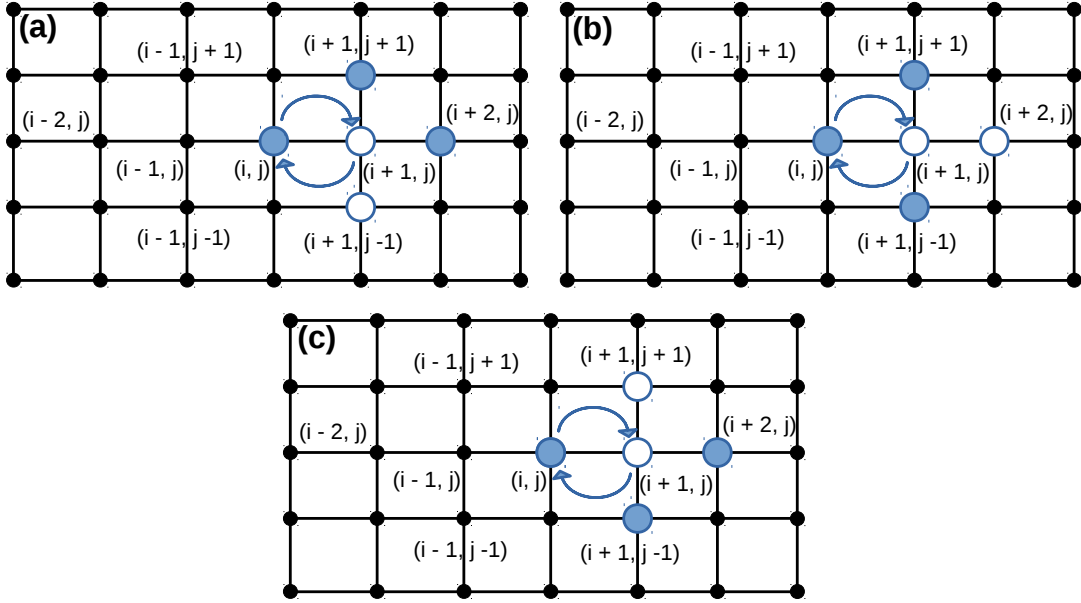


FIG. 4. (Color online) Schematic diagram for a hole at an originating site  $(i, j)$  hopping to its NN site (the intermediate site) and coming back (when any one of the NN sites of the intermediate site is occupied by an electron). Depiction of a hole at  $(i, j)$  jumping to its right NN at  $(i + 1, j)$  and coming back when a particle occupies (a) downward NN of the intermediate site; (b) right NN of the intermediate site; (c) upward NN of the intermediate site. A hole is represented by a blue solid circle whereas a particle by a blue empty circle. All lattice sites that are not relevant to the consideration are indicated by black solid circles.

all the possibilities, similar to and corresponding to Fig. 4, is given by

$$\begin{aligned}
H_3^{(2)} = & -\frac{t^2}{(2E_p + 6V_p)} \sum_{i,j} \left[ \cos^2 \left( \frac{\theta_{i,j;i+1,j}}{2} \right) \left\{ n_{i,j}(1 - n_{i+1,j})n_{i+2,j}n_{i+1,j+1}(1 - n_{i+1,j-1}) \right. \right. \\
& + n_{i,j}(1 - n_{i+1,j})(1 - n_{i+2,j})n_{i+1,j+1}n_{i+1,j-1} + n_{i,j}(1 - n_{i+1,j})n_{i+2,j}(1 - n_{i+1,j+1})n_{i+1,j-1} \left. \right\} \\
& + \cos^2 \left( \frac{\theta_{i,j;i-1,j}}{2} \right) \left\{ n_{i,j}(1 - n_{i-1,j})n_{i-2,j}n_{i-1,j+1}(1 - n_{i-1,j-1}) \right. \\
& + n_{i,j}(1 - n_{i-1,j})(1 - n_{i-2,j})n_{i-1,j+1}n_{i-1,j-1} + n_{i,j}(1 - n_{i-1,j})n_{i-2,j}(1 - n_{i-1,j+1})n_{i-1,j-1} \left. \right\} \\
& + \cos^2 \left( \frac{\theta_{i,j;i,j+1}}{2} \right) \left\{ n_{i,j}(1 - n_{i,j+1})n_{i,j+2}(1 - n_{i-1,j+1})n_{i+1,j+1} \right. \\
& + n_{i,j}(1 - n_{i,j+1})(1 - n_{i,j+2})n_{i-1,j+1}n_{i+1,j+1} + n_{i,j}(1 - n_{i,j+1})n_{i,j+2}n_{i-1,j+1}(1 - n_{i+1,j+1}) \left. \right\} \\
& + \cos^2 \left( \frac{\theta_{i,j;i,j-1}}{2} \right) \left\{ n_{i,j}(1 - n_{i,j-1})n_{i,j-2}n_{i-1,j-1}(1 - n_{i+1,j-1}) \right. \\
& \left. \left. + n_{i,j}(1 - n_{i,j-1})(1 - n_{i,j-2})n_{i-1,j-1}n_{i+1,j-1} + n_{i,j}(1 - n_{i,j-1})n_{i,j-2}(1 - n_{i-1,j-1})n_{i+1,j-1} \right\} \right] \quad (10)
\end{aligned}$$

#### D. All the NN sites of the intermediate site have holes

Here, for the situation where all the NN sites of the intermediate site have holes, we depict in Fig. 5 a hole hopping to an intermediate site and coming back. Here, the coefficient of the second order perturbation term is  $\frac{t^2}{2E_p + 8V_p}$  and

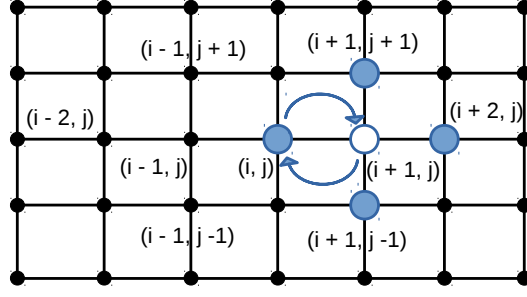


FIG. 5. (Color online) Schematic diagram for a hole at an originating site  $(i, j)$  hopping to its NN site (the intermediate site) and coming back (when all the other three NN sites of the intermediate site are occupied by electrons). Representation of a hole at  $(i, j)$  jumping to its right NN at  $(i + 1, j)$  and coming back. A hole is represented by a blue solid circle and a particle by a blue empty circle. All lattice sites irrelevant to the analysis are represented by black solid circles.

the contribution to  $H^{(2)}$  from all the possibilities, similar to and corresponding to Fig. 5, is given by

$$\begin{aligned}
 H_4^{(2)} = & -\frac{t^2}{(2E_p + 8V_p)} \sum_{i,j} \left[ \cos^2 \left( \frac{\theta_{i,j;i+1,j}}{2} \right) \left\{ n_{i,j} (1 - n_{i+1,j}) n_{i+2,j} n_{i+1,j+1} n_{i+1,j-1} \right\} \right. \\
 & + \cos^2 \left( \frac{\theta_{i,j;i-1,j}}{2} \right) \left\{ n_{i,j} (1 - n_{i-1,j}) n_{i-2,j} n_{i-1,j+1} n_{i-1,j-1} \right\} \\
 & + \cos^2 \left( \frac{\theta_{i,j;i,j+1}}{2} \right) \left\{ n_{i,j} (1 - n_{i,j+1}) n_{i,j+2} n_{i-1,j+1} n_{i+1,j+1} \right\} \\
 & \left. + \cos^2 \left( \frac{\theta_{i,j;i,j-1}}{2} \right) \left\{ n_{i,j} (1 - n_{i,j-1}) n_{i,j-2} n_{i-1,j-1} n_{i+1,j-1} \right\} \right]. \quad (11)
 \end{aligned}$$

From the contributions  $H_1^{(2)}$ ,  $H_2^{(2)}$ ,  $H_3^{(2)}$ , and  $H_4^{(2)}$  obtained above, we express  $H^{(2)}$  as

$$H^{(2)} = H_1^{(2)} + H_2^{(2)} + H_3^{(2)} + H_4^{(2)}. \quad (12)$$

Lastly, the superexchange<sup>27</sup> term  $H_{SE}$  generates A-AFM spin-spin exchange in manganites such as  $\text{LaMnO}_3$  and is given by

$$H_{SE} = -J_{xy} \sum_{\langle i,j \rangle_{xy}} \cos(\theta_{ij}) + J_z \sum_{\langle i,j \rangle_z} \cos(\theta_{ij}). \quad (13)$$

It is important to note that, while the range of charge-charge interaction is as far as NNNN, the range of spin-spin interaction is only NN.

### III. CALCULATION PROCEDURE

For a numerical study, we consider a 2D lattice with periodic boundary conditions in both directions. We treat the problem fully classically using the effective Hamiltonian, comprising of the effective electron-phonon interaction (the charge-spin-coupled term) and the superexchange interaction (the spin-spin interaction term), as given by Eq. (7). We use classical Monte Carlo technique and make use of the standard Metropolis algorithm to

update the charge configuration as well as the spin configuration of the system. We follow a two-step procedure to arrive at the final charge and spin configurations.

Firstly, to deal with problem of charge configurations that correspond to local minima which are close in energy, we take resort to simulated annealing for the charge degrees of freedom only. The spin variables are kept frozen since the energy scale for the charge interactions is much higher than the energy scale for superexchange interactions. Since we are working with low hole densities (i.e., between 0.1 and 0.3), a large number of degenerate states will appear in the charge spectrum. In order to obtain maximum number of such degenerate configurations, we employ a three-step procedure at each temperature of the simulated annealing process to obtain the optimized charge configurations. The primary step is a “single-particle-exchange” process where we choose any two sites at a time—one sequentially and the other randomly—and exchange their number density values provided they differ by 1. Physically we exchange a particle at a site with a hole at any other site. The secondary step is a “general-two-particle-exchange” process where any two random sites are selected with both being occupied by particles and then their occupants are exchanged with another pair of randomly chosen sites both containing holes. Thus we actually exchange two particles

with two holes at a time. The final step—a “plaquette-exchange” process—is a special case of the “general-two-particle-exchange” mechanism. Here plaquette are chosen sequentially; if the difference in number densities between the two diagonal pairs is 2, then the number densities of the diagonals are exchanged. At a particular temperature, to arrive at the final lowest energy charge configuration at that temperature using Monte Carlo technique, an initial random charge configuration (with a fixed number of particles) first goes through  $4 \times 10^5$  steps of “single-particle-exchange”; then an equal number of steps involving “general-two-particle-exchange”; followed by 30 times the system size number “plaquette-exchange” steps.

Secondly, using the charge profile generated by the three-step process, we now optimize spin variables by taking an initial random spin configuration and updating through the Metropolis algorithm. The spins being large in magnitude, with  $S = 2$ , are essentially classical spins with  $\vec{S}_i = (\sin \theta_i \cos \phi_i, \sin \theta_i \sin \phi_i, \cos \theta_i)$ . While updating the spins, we consider the full Hamiltonian  $H_{\text{eff}}$  and consider both the charge and spin interaction energies. The  $\cos(\theta)$  and  $\phi$  values are binned to fix the orientation of the classical spin vector. We have allowed equally spaced 40 values of  $\cos(\theta)$  in the interval  $(-1, 1)$  and 80 values of  $\phi$  in the usual range of  $(0, 2\pi)$ , thus totaling to 3200 different possibilities. A sweep involves visiting all the lattice sites sequentially and updating the spin orientation at each lattice site by the Metropolis algorithm. The equilibrium number of sweeps required for medium (higher) temperatures is around  $15 \times 10^5$  ( $6 \times 10^5$ ), while another  $15 \times 10^5$  ( $6 \times 10^5$ ) sweeps are required for the thermal averaging of the total magnetization of the system. It is to be noted that for low hole concentrations, we have many degenerate states. We calculate the magnetization for typically 10 degenerate configurations. The degenerate states are chosen based on the charge optimization process only, fed to the full Hamiltonian  $H_{\text{eff}}$  containing both charge and spin variables, and then energy is optimized to obtain the total magnetization of all such states. The magnetization/site of the system, that has been plotted, is the magnetization/site averaged over all the degenerate states for a particular filling of holes when spins normalized to unity.

We study the system for the bare hopping parameter values  $t = 0.2$  eV and  $t = 0.3$  eV. Our calculations take the polaronic energy to be  $E_p = 0.43$  eV and the nearest-neighbor repulsion energy to be  $V_p = 0.07$  eV. Thus, we are in the regime of strong electron-phonon coupling characterized by  $(E_p + V_p)/\omega_0 \gg 1$  with the optical phonon frequency  $\omega_0$  value being given as  $0.05$  eV  $< \omega_0 < 0.1$  eV. The superexchange energy coefficient  $J_z = 4.8$  meV<sup>23,24</sup>; thus the superexchange energy is much smaller than the electron-hole pair ferromagnetic interaction coupling  $[t^2/(2E_p + 2V_p)]$ . Furthermore, the ferromagnetic coupling  $J_{xy} = 1.4 \times J_z$ . Thus, the charge configuration can be assumed to remain constant as the spins are optimized. The total magnetization of the system is computed at various temperatures, with the high-

est temperature being  $T = 0.1t/k_B$  (i.e., about 330K for  $t = 0.3$  eV. Henceforth,  $k_B$  will be set to unity for convenience.. The lowest temperature on the other hand is  $T = 0.001t$  (i.e., about 3K for  $t = 0.3$  eV) which is much smaller than  $J_z$ ; thus, the system can be assumed to be in its ground state at  $T = 0.001t$ . Here, we should comment that above  $T = 0.03t$ , the excited-state charge configurations also begin to contribute to the magnetization.

## IV. RESULTS AND DISCUSSION

We consider a 2D lattice of dimensions  $6 \times 12$ , (i.e., with a total of 72 sites) with periodic boundary conditions in both directions; the number of rows being  $l_x = 6$  and the number of columns being  $l_y = 12$ . Each site represents an Mn ion consisting of an electron and a positive charge center. We study the interplay between the electron-phonon interaction and the magnetic interaction of the spins [see Eq. (7)]. As stated earlier (in Sec. I), due to the smallness of the kinetic energy in comparison to the potential energy, the problem is treated fully classically. Thus the holes are site-localized and the system can be represented by a single state in the occupation number basis with the number density at each site being either 1 or 0. Hence, for strong electron-phonon interaction, we have a fully insulating system resembling a charge solid as shown in Fig. 7. Using effective Hamiltonian in Eq. (7), we can simulate different observables in the system. We study the variation of the total magnetization of the system as a function of hole doping in the pure manganite sample.

### A. A-AFM background

The hopping value  $t$  is varied to study the interplay between the electron-phonon interactions and the superexchange interactions in the system. The hole doping  $x$  is varied as  $0.1 \leq x \leq 0.3$ . The magnetic profile still resembles that of an A-AFM system away from the holes; in the NN vicinity of a hole, the spins get polarized in the direction of the spin of the hole thereby forming a magnetic polaron. For different hopping cases, the temperature variation of the total magnetization of the system is studied. We have also considered a 2D lattice with system size  $12 \times 12$  and carried out the magnetization measurements. It shows qualitatively similar results as that of the  $6 \times 12$  lattice as depicted in Fig. 6. However, the  $12 \times 12$  system requires a running time which is  $\simeq 5$  times that of the  $6 \times 12$  case; also, the number of degenerate states for the  $12 \times 12$  system is much more. Thus, dealing with the  $12 \times 12$  case is computationally expensive. So, we conclude that  $6 \times 12$  lattice can be considered to be representative for the  $12 \times 12$  lattice and will be used for investigating the ferromagnet-insulator properties of the system.



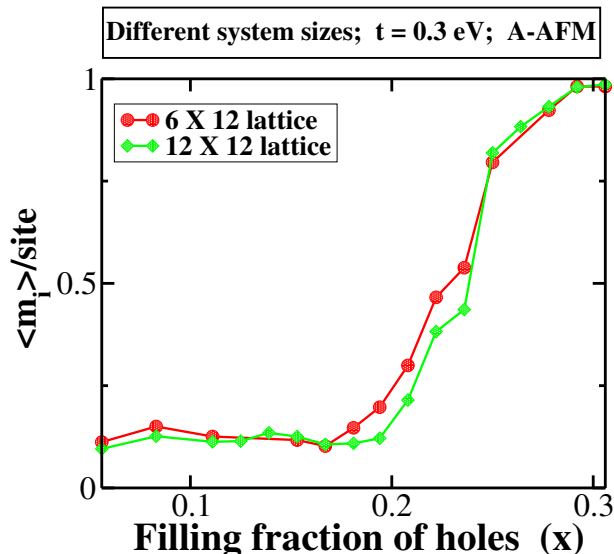


FIG. 6. (Color online) Averaged per-site magnetization  $\langle m_i \rangle$  (of spins normalized to unity) as a function of hole doping  $x$  for two different lattices ( $6 \times 12$  and  $12 \times 12$ ) and for a fixed  $T = 0.001t$ .

At a very low-hole concentration  $\simeq 0.1$  (i.e., 8 particles on a 72-site lattice), 8 holes get distributed among 12 columns such that NN as well as NNN and NNNN interactions are avoided. In most of the degenerate states, no two holes occupy the same column. Hence we have site-localized holes in the system, polarizing their NN spins, giving rise to magnetic polarons that remain disconnected in the lattice. Due to the NN interaction  $J_{xy}$ , spins in a column try to align ferromagnetically. Thus, the ferromagnetic polarons and the ferromagnetic interaction in columns together give rise to an effective low magnetization value (with a sizeable fluctuation).

At each temperature, the value of magnetization is essentially unchanged between hole densities  $8/72$  and  $12/72$  ( $\simeq 0.167$ ); this is because up to the filling  $12/72$ , holes can still maintain to be non-interacting (on ignoring the superexchange) as can be seen in Fig. 7 (a).

At temperatures  $T < J_z$  ( $= 0.016t$  for  $t = 0.3$  eV and  $= 0.024t$  for  $t = 0.2$  eV), antiferromagnetic coupling between columns is effective and the system has low magnetization at low concentrations (i.e.,  $x \leq 12/72$ ). On increasing the temperature up to  $T = J_z$ , the effect of  $J_z$  diminishes while the effect of ferromagnetic coupling  $J_{xy} = 1.4J_z$  is more dominant; thus, magnetism in the system increases with increasing temperature. For higher temperatures  $T > J_{xy}$  and again at low concentrations (i.e.,  $x \leq 12/72$ ), the effect of the ferromagnetic coupling  $J_{xy}$  also diminishes, and the magnetism decreases with increasing temperature.

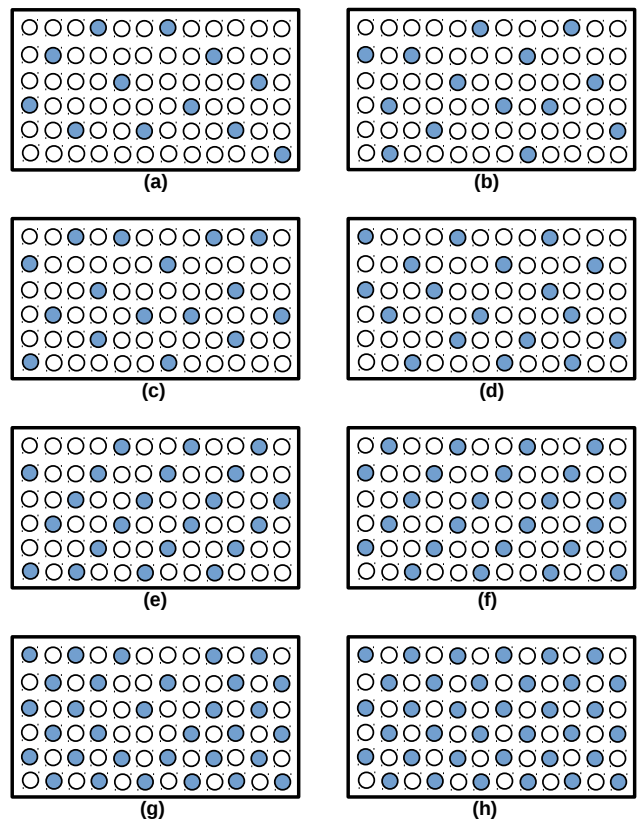


FIG. 7. (Color online) Charge configurations in the ground state of a  $6 \times 12$  lattice. An arbitrarily chosen degenerate ground state, involving 72 sites, for (a) 12 holes, (b) 14 holes, (c) 16 holes, (d) 18 holes, (e) 22 holes, (f) 24 holes (diagonal stripe order), (g) 32 holes, and (h) 36 holes.

### 1. $t=0.3$ eV case

As the concentration of holes increases, initially NNNN interactions and later NNN interactions become relevant; the NN interactions being the strongest are still avoided. Thus longer ferromagnetic chains are formed, thereby increasing the total magnetization of the system. So by  $x = 14/72 \simeq 0.194$  [see Fig. 7 (b)], magnetization for lower temperatures such as  $T = 0.001t$  starts rising sizeably; the peak magnetization value is now at a reduced temperature of  $T = 0.01t$ . By  $x = 18/72 = 0.25$  [see Fig. 7 (d)] NNN interactions also appear, the different local magnetic polarons start interacting with one another and hence form larger magnetic polarons and the peak magnetization temperature reduces to  $T=0.001t$ ; here, starting from  $T = 0.1t$ , the magnetization increases with decreasing temperature. It is to be noted that there occurs a narrow crossover region ( $14/72 \leq x \leq 17/72$ ) where magnetization curves for different temperatures intersect. In the crossover regime, there is a complex interplay of various competing effects: 1) aligning of different magnetic polarons due to dominance of  $J_{xy}$  over  $J_z$ ; 2) reduction of electron-hole spin interactions due to appearance

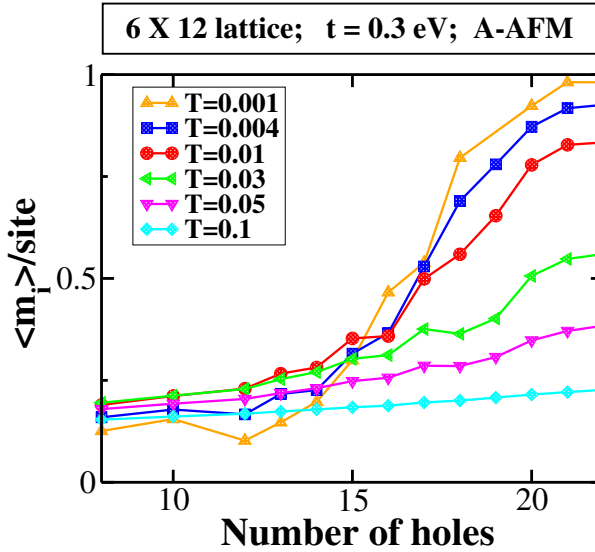


FIG. 8. (Color online) Averaged per-site total magnetization  $\langle m_i \rangle$  (of spins normalized to unity) as a function of the number of holes doped for a  $6 \times 12$  lattice and for various temperatures (expressed in units of hopping parameter  $t$ ). The background spin configuration is A-AFM type and hopping  $t = 0.3$  eV.

of NNNN and NNN interactions (of strength  $\frac{t^2}{2E_p+4V_p}$ ); 3) commencing of percolation effects of magnetic polarons due to large hole concentrations; and 4) disordering effects of the temperature. At  $x = 18/72$  ( $= 0.25$ ), percolation effect of magnetic polarons is largely dominant over antiferromagnetic interactions. At even higher hole concentrations, this effect is even more pronounced; magnetization rises faster with lowering of temperature. As can be seen from Fig. 8, at lower temperatures and for  $x > 15/72$ , the magnetization increases faster with increasing hole concentration. At  $T = 0.001t$ , we get an almost fully ferromagnetic large cluster for  $x = 22/72 \simeq 0.3$  [see Fig. 7 (e)], with averaged magnetization values close to the maximum possible.

## 2. $t=0.2$ eV case

For the  $t = 0.2$  eV situation, the crossover region (i.e.,  $13/72 \leq x \leq 19/72$ ) is wider than it is for the  $t = 0.3$  eV case. The peak-magnetization temperature oscillates in the crossover regime (see Fig. 9); furthermore, the curves corresponding to  $T \lesssim J_z = 0.024t$  intersect more than once in the crossover region. A plausible explanation for this can be given as follows. The ratio of electron-hole spin interaction and antiferromagnetic coupling  $\left[\left(\frac{t^2}{2E_p+2V_p}\right)/J_z\right]$  is only 8; when NNN and NNNN interactions are relevant, the ratio reduces to  $\left(\frac{t^2}{2E_p+4V_p}\right)/J_z = 7$ . Thus antiferromagnetic coupling becomes more prominent than for the  $t = 0.3$  eV case and frustration effects become relevant. It could be

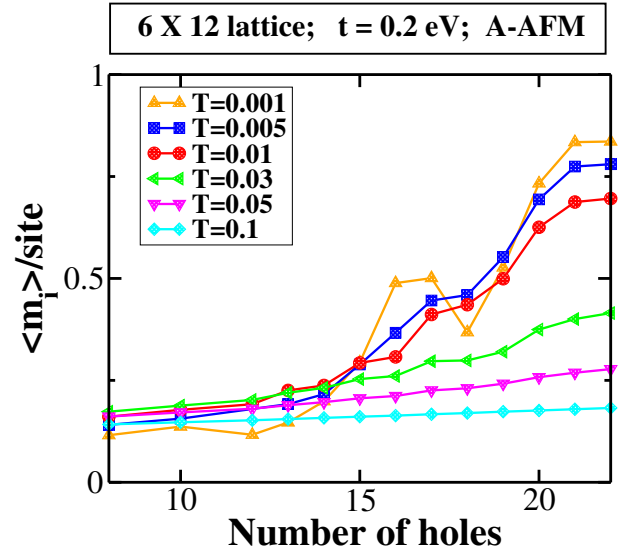


FIG. 9. (Color online) Averaged per-site total magnetization  $\langle m_i \rangle$  (of spins normalized to unity) as a function of the number of holes doped for a  $6 \times 12$  lattice and for various temperatures (in units of hopping  $t$ ). The background spin configuration is A-AFM and  $t = 0.2$  eV.

due to frustration that, at lower temperatures (such as  $T = 0.001t$ ), the magnetization curve drops at the higher carrier concentration  $x = 18/72 = 0.25$ . This also could be an indication of the superspin glass phase claimed in experiments<sup>19</sup>; here, “superspin” refers to a spin cluster (i.e., a large magnetic polaron). At  $x \geq 20/72$  ( $\simeq 0.28$ ), percolation effect of magnetic polarons dominates over antiferromagnetic interactions; magnetization rises with lowering of temperature. Finally, for the higher hole concentration  $x = 22/72 \simeq 0.3$  and at  $T = 0.001t$ , we get a reasonably high magnetization value of 0.85.

## B. G-AFM background, $t=0.3$ eV case

To gain further insight, we study the interplay between the strong ferromagnetic electron-hole interaction that polarizes the NN spins of a hole and the superexchange NN antiferromagnetic interaction  $J_z$ . The magnetic profile, away from the holes, resembles that of a G-AFM system; the holes form ferromagnetic polarons involving the hole spin and the NN spins. At temperatures  $T \lesssim J_z = 0.016t$  and hole fillings up to  $x = 24/72$ , due to the effect of antiferromagnetic  $J_z$  coupling on all sides, the polarizations of the magnetic polarons oppose each other leading to a low magnetization as shown in Fig. 10. For higher temperatures, due to the dominance of the disordering effect of the temperature over the superexchange interaction, there is a probability for the clusters to get less misaligned. Hence we notice an increase in the magnetization for  $T > J_z$ . For  $x = 24/72 = 1/3$ , we have a diagonal stripe order as depicted in Fig. 7 (f); each column has two holes. For this arrangement, diagonals

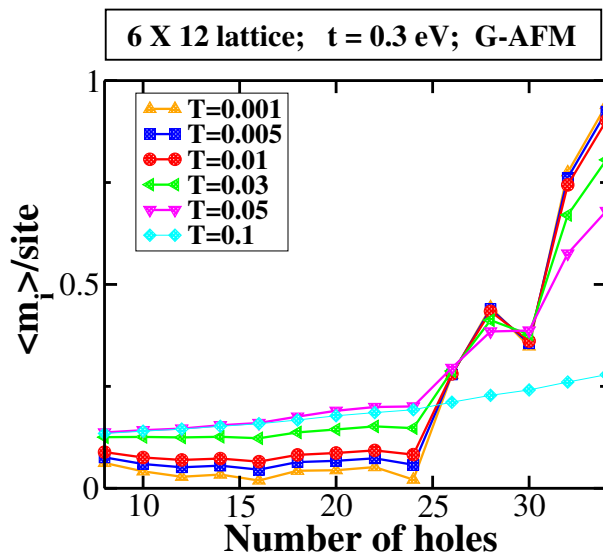


FIG. 10. (Color online) Averaged per-site total magnetization  $\langle m_i \rangle$  (of spins normalized to unity) as a function of the number of holes doped for a  $6 \times 12$  lattice and for various fixed temperatures (in units of hopping parameter  $t$ ). The background spin configuration is G-AFM type and  $t = 0.3$  eV.

containing holes are ferromagnetic, but every such diagonal (with holes) is antiferromagnetically coupled to its neighboring diagonal. In each column, half the spins are in one direction while the other half are in the opposite direction leading to a very small total magnetization.

Here too, very similar to the case of  $t = 0.2$  eV with A-AFM background, there is a crossover region; the crossover occurs in the region  $24/72 < x < 32/72$ . In the crossover regime, the peak-magnetization temperature oscillates and the curves for  $T \lesssim Jz$  intersect thrice in the crossover region. Since all the background spins interact antiferromagnetically (which is in contrast to the A-AFM case), percolation of magnetic polarons dominates over antiferromagnetic interactions at an even larger filling; around  $x \geq 32/72 = 0.44$  [refer Fig. 7 (g)], magnetization increases with lowering of temperature.. It is to be noted that, for half-filling [see Fig. 7 (h)], we should expect a fully ferromagnetic spin profile with a checkerboard charge structure.<sup>20</sup>

### C. Fully FM background, $t=0.3$ eV

Lastly, to better appreciate subtleties pertaining to FMI, we also study the case where the superexchange interaction is fully ferromagnetic (FM) with coupling  $J_z = 0.016t$  when  $t = 0.3$  eV. Here, while in the NN vicinity of a hole the spins get strongly polarized thereby forming a ferromagnetic magnetic polaron, the magnetic profile is that of a weaker FM system away from the holes. Hence, for temperatures much smaller than  $J_z$  (such as  $T = 0.001t$ ), we have an almost fully ferromagnetic sys-

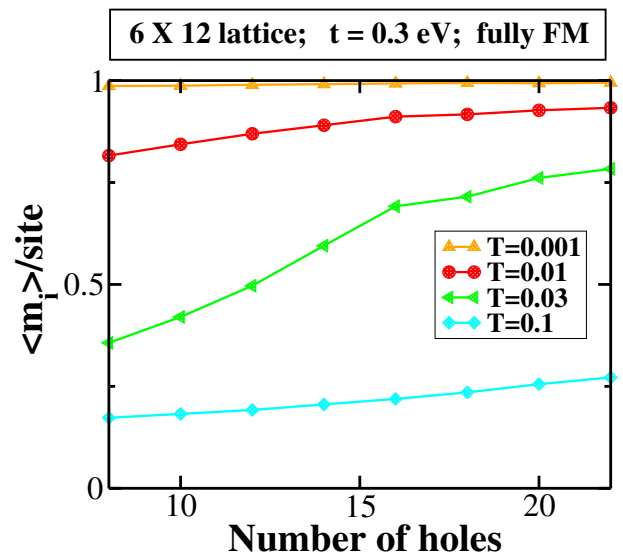


FIG. 11. (Color online) Averaged per-site total magnetization  $\langle m_i \rangle$  (of spins normalized to unity) as a function of the number of holes doped for a  $6 \times 12$  lattice and for various fixed temperatures (in units of hopping parameter  $t$ ). The background spin configuration is fully FM and  $t = 0.3$  eV.

tem as shown in Fig. 11, On increasing the temperature, the spins get more misaligned and the magnetization reduces. At lower fillings, as the temperature increases to the value  $0.03t$  (i.e.,  $T \approx 2J_z$ ), the disordering effect is large enough so that the magnetization drops considerably as shown in Fig. 11; On the other hand, at higher fillings and again at  $T = 0.03t$ , percolation of magnetic polarons counters the disordering effect and generates higher magnetization values. For still higher temperatures (such as  $T = 0.1t$ ), the magnetic polarons tend to orient in random directions because the superexchange coupling is ineffective, thereby reducing the magnetization significantly. It is interesting to note that, in all the three Figs. 8, 10, and 11 plotted at  $t = 0.3$  eV, the magnetization curves are similar because the superexchange is ineffective and hence the nature of superexchange coupling is irrelevant.

## V. CONCLUSIONS AND PERSPECTIVES

We studied the nature of ferromagnetic insulator in the experimentally relevant doping regime of  $0.1 \leq x \leq 0.3$  in bulk manganites. The magnetic interaction considered here applies to manganites with low density of localized holes. In regions without holes, as in the undoped manganites, the magnetic interaction is A-AFM; in a region with a hole, the site-localized hole produces strong ferromagnetic coupling between its spin and its NN electron spins. We find that near the doping  $x = 0.3$ , the insulator is almost fully ferromagnetic. Now, the critical doping at which the system becomes fully ferromagnetic depends on the dimension; in 2D it is expected to be around

twice the value of the critical doping in three dimensions (3D) for the following reason. In a conducting-site percolation problem, the critical concentration for conduction in a simple cubic lattice is 0.31 and in a square lattice it is 0.59 [see Ref. 30]; hence, the critical doping to produce a percolating cluster that is a checkerboard charge-ordered region is  $0.5 \times 0.31$  in 3D and at  $0.5 \times 0.59$  in 2D [see Ref. 31].

It was experimentally observed that a FMI phase is manifested in the wide-band manganite  $\text{La}_{1-x}\text{Sr}_x\text{MnO}_3$  in the doping region  $0.1 \lesssim x \lesssim 0.18$ <sup>21</sup>, in the intermediate-bandwidth  $\text{La}_{1-x}\text{Ca}_x\text{MnO}_3$  in the doping range  $0.1 \leq x \leq 0.225$ <sup>21,22</sup>, and in the narrow-bandwidth  $\text{Pr}_{1-x}\text{Ca}_x\text{MnO}_3$  in the region  $0.1 \leq x \leq 0.3$ <sup>21</sup>. The fact that the FMI region persists till a higher doping when bandwidth decreases (and concomitantly electron-phonon coupling increases<sup>15</sup>) is consistent with the fact that the tendency to localize increases as bandwidth decreases<sup>17,18</sup>. The hopping values considered in this work are pertinent to wide-bandwidth and intermediate-bandwidth manganites. While our one-band model (involving site-localized holes) is relevant to understand manganites in the FMI region, it is certainly not valid to study the ferromagnet metallic (FMM) phase that occurs at higher doping in manganites; to understand the FMM region, we need to invoke a two-band model and/or

analyze the effect of disorder on localization.

The experimental managanite phase diagram reported in Ref. 32 reveals increasing  $T_c$  values at higher dopings for the FMI phase in  $\text{La}_{1-x}\text{Sr}_x\text{MnO}_3$ . Based on this phase diagram, for a fixed  $T < T_c(x = 0.1)$ , we expect the magnetization to increase when the doping increases in the FMI region; this is consistent with the curves in Fig. 8.

Lastly, comparing the  $t = 0.2$  eV, A-AFM case with the  $t = 0.3$  eV, G-AFM case, we conclude that the antiferromagnetic coupling  $J_z$  plays the important role of causing frustrations in the system. We also point out the possible occurrence of glassiness in the system to explain the multiple intersections of the curves in the crossover regime at  $T \lesssim J_z$  (see Figs. 9 and 10). Such a picture is supported by the observed superspin glass phase in  $\text{La}_{0.82}\text{Ca}_{0.18}\text{MnO}_3$  ferromagnetic insulator at  $T \lesssim 70$  K<sup>19</sup>. Further theoretical analysis is required to clearly identify and characterize a superspin glass phase at lower temperatures.

## VI. ACKNOWLEDGEMENTS

The authors would like to thank A. Ghosh and P. B. Littlewood for useful discussions.

- 
- <sup>1</sup> *Colossal Magnetoresistance, Charge Ordering, and Related Properties of Manganese Oxides*, edited by C.N.R. Rao and B. Raveau (World Scientific, Singapore, 1998).
- <sup>2</sup> D. I. Khomskii, *Physica Scripta* **72**, CC8-14 (2005).
- <sup>3</sup> T. Hotta, *Rep. Prog. Phys.* **69**, 2061 (2006).
- <sup>4</sup> Y. Tokura, *Rep. Prog. Phys.* **69**, 797 (2006).
- <sup>5</sup> See K.H. Kim, M. Uehara, V. Kiryukhin and S.-W. Cheong, in *Colossal Magnetoresistive Manganites*, edited by T. Chatterji, (Kluwer Academic, Dordrecht, 2004).
- <sup>6</sup> C. Martin, A. Maignan, M. Hervieu, and B. Raveau, *Phys. Rev. B* **60**, 12191 (1999).
- <sup>7</sup> A. J. Millis, P. B. Littlewood, and B. I. Shraiman, *Phys. Rev. Lett.* **74**, 5144 (1995).
- <sup>8</sup> Sanjeev Kumar and Pinaki Majumdar, *Phys. Rev. Lett.* **96**, 016602 (2006); S. Kumar and P. Majumdar, *cond-mat* 0406082.
- <sup>9</sup> A. Ghosh and S. Yarlagadda, *Phys. Rev. B* **96**, 125108 (2017).
- <sup>10</sup> P. C. Dai, J. A. Fernandez-Baca, E. W. Plummer, Y. Tomioka, and Y. Tokura, *Phys. Rev. B* **64**, 224429 (2001).
- <sup>11</sup> P. C. Dai, J. A. Fernandez-Baca, N. Wakabayashi, E. W. Plummer, Y. Tomioka, and Y. Tokura, *Phys. Rev. Lett.* **85**, 2553 (2000).
- <sup>12</sup> W. Jiang, X. Z. Zhou, G. Williams, R. Privezentsev, and Y. Mukovskii, *Phys. Rev. B* **79**, 214433 (2009).
- <sup>13</sup> V. Markovich, E. Rozenberg, A. I. Shames, G. Gorodetsky, I. Fita, K. Suzuki, R. Puzniak, D. A. Shulyatev, and Y. M. Mukovskii, *Phys. Rev. B* **65**, 144402 (2002).
- <sup>14</sup> V. Markovich, I. Fita, R. Puzniak, M. I. Tsindlekht, A. Wisniewski, and G. Gorodetsky, *Phys. Rev. B* **66**, 094409 (2002).
- <sup>15</sup> T. F. Seman, K. H. Ahn, T. Lookman, A. Saxena, A. R. Bishop, and P. B. Littlewood, *Phys. Rev. B* **86**, 184106 (2012).
- <sup>16</sup> G. G. Guzmán-Verri, R. T. Brierley, P. B. Littlewood, e-print arXiv:1701.02318.
- <sup>17</sup> G. V. Pai, S. R. Hassan, H. R. Krishnamurthy, and T. V. Ramakrishnan, *Europhys. Lett.* **64**, 696 (2003); T. V. Ramakrishnan, H. R. Krishnamurthy, S. R. Hassan, and G. V. Pai, *Phys. Rev. Lett.* **92**, 157203 (2004).
- <sup>18</sup> M. Yu. Kagan, D. I. Khomskii, and M.V. Mostovoy, *Eur. Phys. J. B* **12**, 217 (1999).
- <sup>19</sup> P. A. Kumar, R. Mathieu, P. Nordblad, S. Ray, O. Karis, G. Andersson, and D. D. Sarma, *Phys. Rev. X* **4**, 011037 (2014).
- <sup>20</sup> S. Paul, R. Pankaj, S. Yarlagadda, P. Majumdar, and P. B. Littlewood, *Phys. Rev. B* **96**, 195130 (2017).
- <sup>21</sup> V. Markovich, A. Wisniewski, and H. Szymczak, Magnetic properties of perovskite manganites and their modifications, in *Handbook of Magnetic Materials* **22**, 1-201 (2014), edited by K. H. J. Buschow (New York: Elsevier).
- <sup>22</sup> P. Schiffer, A. P. Ramirez, W. Bao, and S.-W. Cheong, *Phys. Rev. Lett.* **75**, 3336 (1995).
- <sup>23</sup> K. Hirota, N. Kaneko, A. Nishizawa, and Y. Endoh, *J. Phys. Soc. Jpn.* **65**, 3736 (1996); F. Moussa, M. Hennion, J. Rodríguez-Carvajal, H. Moudden, L. Pinsard, and A. Revcolevschi, *Phys. Rev. B* **54**, 15149 (1996); G. Biotteau, M. Hennion, F. Moussa, J. Rodríguez-Carvajal, L. Pinsard, A. Revcolevschi, Y. M. Mukovskii, and D. Shulyatev, *ibid.* **64**, 104421 (2001).
- <sup>24</sup> N. N. Kovaleva, Andrzej M. Oleś, A. M. Balbashov, A. Maljuk, D. N. Argyriou, G. Khaliullin, and B. Keimer,

- Phys. Rev. B **81**, 235130 (2010).
- <sup>25</sup> P. -G. de Gennes, Phys. Rev. **118**, 141 (1960).
- <sup>26</sup> Y. A. Izyumov, Y. N. Skryabin, Phys.-Usp. **44**, 109 (2001).
- <sup>27</sup> P. W. Anderson, Phys. Rev. **115**, 2 (1959).
- <sup>28</sup> R. Pankaj and S. Yarlagadda, Phys. Rev. B **86**, 035453 (2012)
- <sup>29</sup> A. Dey, M. Q. Lone, and S. Yarlagadda, Phys. Rev. B **92**, 094302 (2015).
- <sup>30</sup> A. L. Efros, *Physics and Geometry of Disorder* (Mir Publishers, Moscow, 1986).
- <sup>31</sup> S. Datta and S. Yarlagadda, Proceedings of the DAE Solid State Physics Symposium (Golden Jubilee) **50**, 605 (2005).
- <sup>32</sup> A. Urushibara, Y. Moritomo, T. Arima, A. Asamitsu, G. Kido, and Y. Tokura Phys. Rev. B **51**, 14103 (1995).